IEEE Access
Multidisciplinary | Rapid Review | Open Access Journal

Received October 3, 2019, accepted November 25, 2019, date of publication December 10, 2019,
date of current version December 23, 2019.

Digital Object Identifier 10.1109/ACCESS.2019.2958835

LoRa-Based Precision Wireless Structural Health Monitoring System for Bolted Joints in a Smart City Environment

MICHAIL SIDOROV[1], PHAN VIET NHUT[2], YUKIHIRO MATSUMOTO[2], AND REN OHMURA[1]
[1]Department of Computer Science and Engineering, Toyohashi University of Technology, Toyohashi 441-8580, Japan
[2]Department of Architecture and Civil Engineering, Toyohashi University of Technology, Toyohashi 441-8580, Japan

Corresponding author: Michail Sidorov (michail.sidorov.cl@tut.jp)

ABSTRACT Smart City is a cutting edge technology driven city aimed at making our everyday lives safer and more convenient. Like every city it is comprised of structures. To uphold their safety these structures have to undergo periodical maintenance checks. However, checks are done manually, thus consume a significant amount of time and financial resources. Remote Structural Health Monitoring (RSHM) is a perfect solution for a Smart City, however limited research is done in applying Internet of Things (IoT) sensor nodes for permanent RSHM in applications that use bolted joints as a main fastening method. Most of the proposed solutions are not suitable, since either additional structural modifications are required, they violate standards, provide poor wireless communication range or still require human intervention. Therefore, this paper proposes an IoT sensor node named TenSense M30, which leverages Long Range (LoRa) communication technology to enable wide communication coverage and long life for monitoring the health of bolted joints in a Smart City environment. TenSense M30 has a miniature footprint and can be used as an add-on to current structures. Mechanical, hardware and embedded designs are presented and evaluated by means of simulation and practical tests. Results show that TenSense M30 is capable of precisely monitoring the pre-tension load of bolted joints, has a secured non-line of sight communication channel with a distance of 800 meters, has an expected lifetime of greater than 5 years powered by a number of coin cell batteries, and is safe under the pre-tension load.

INDEX TERMS Strain measurement, Internet of Things, sensor systems and applications, remote monitoring, bolted joint, LoRa.

I. INTRODUCTION

The concept or a vision of a smart city consists of multiple disciplines and infrastructures intertwined together. Although the full picture is still unclear, it was already discussed in numerous papers from different perspectives [1]–[4]. The general consensus is that the driving force behind the notion of a smart city is the Internet of Things (IoT), since the ''smart'' part can be mostly realized with the help of numerous sensor nodes gathering the data and feeding it to various software algorithms that help to determine further actions. The purpose of a smart city is very simple - to make the daily living easier, safer and more convenient for its inhabitants. Although the purpose is clear there are numerous challenges standing before realizing the concept, which are very diverse in nature and include but not limited to the cost of implementation and operation of the city, efficiency, communication, security, various environmental, social and economic factors, etc. The concept of the smart city is visualised in Fig. 1.

The core components of a smart city are mostly driven by technology that is vital to our everyday lives. The major sectors that help to shape the smart city include smart power grid [5], [6], smart healthcare [7], [8], digital identity [9], [10], smart transportation [1], smart buildings, constructions, homes, and factories [11], [12], etc.

Numerous IoT nodes are presented in various papers that can be utilized in a Smart City. However, these are mostly aimed at collecting environmental data, e.g. temperature, humidity, particulates, noise pollution, etc. [2], [3], [9]. There is limited research done in the area of applying IoT sensor

The associate editor coordinating the review of this manuscript and approving it for publication was Razi Iqbal.

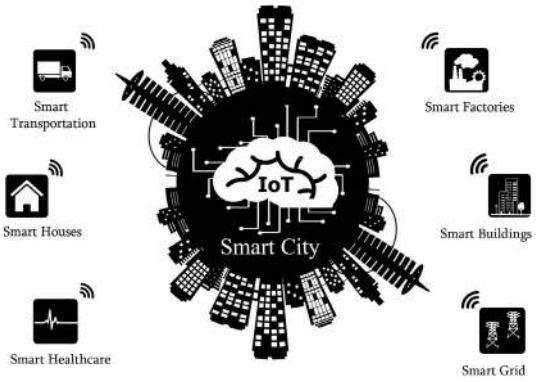

FIGURE 1. Smart city concept and its core components.

nodes for permanent bolted joint Remote Structural Health Monitoring (RSHM), moreover none is conducted for the purpose of integration into a Smart City. Structural Health Monitoring (SHM) is highly relevant to the concept of a Smart City as it can be useful both for Smart Buildings, Constructions, and for Smart Transportation services. Buildings and structures not only have to be smart, but also safe. In order to preserve structural integrity it has to be maintained. This is true for everything that experiences wear and tear, and is forced to degrade due to various environmental conditions. In constructions that utilize a bolted joint as a fastening method this is particularly important.

Bolted joint is an incredibly easy to use fastening method, thus aircrafts, buildings, bridges, offshore structures, etc. all employ it. The fastening method works by clamping two or more objects together using tension. This tension comes from the rotary force applied to the fastener. Once deployed bolted joints experience different kinds of stress which over time can lead to their failure. The usual sources of stress are vibration, shock and thermal expansion. Sometimes fasteners themselves may be susceptible to elongation process due to heavy load applied. Thus, in order to avoid failures scheduled inspections of bolted joints are performed. However, the drawbacks of these inspections are cost, timing and convenience. It may not be convenient to perform inspections with limited access to the structure. Furthermore, it is possible for the fault to develop unnoticed until a critical damage occurs to the bolted joint and subsequently to the structure. This would create a safety issue and result in costly repairs. Thus, in order to prevent unnecessary damage, save time and resources a remote monitoring of a bolted joint is the best solution to this problem.

II. RELEVANT WORK

A number of different sensors can be used for SHM. Most widespread ones for this purpose are:

- Fiber-optic sensors e.g. Fiber Bragg Grating (FBG) strain sensors
- Ultrasonic Guided Wave (UGW) sensors, e.g. Piezoelectric Transducers (PZT)
- Electrical properties sensors: resistance, impedance, dielectric, e.g. strain gauges
- Accelerometers

All of them are used to monitor the changes in a structure over time, albeit using different approaches and mounting techniques. Looking at the techniques used to measure the tension of a bolted joint we can notice that they involve both invasive and non-invasive methods. Invasive methods include making physical modifications to the bolt itself to accommodate the sensing mechanism, e.g. Mekid *et al*. proposed a bolt tension monitoring system requiring the addition of a piezoelectric material inside the core of the bolt [13]. Ohta *et al*. proposed to embed strain gauges inside the bolt to measure tension and send the data wirelessly [14]. These approaches are highly undesirable since the modifications will inevitably negatively impact the properties of the fastener and will force it to deviate from the standards, e.g. ISO, ANSI, ASME, etc. leading the whole structure not to conform to safety requirements. Thus, non-invasive methods are preferred, e.g. Smith *et al*. proposed a tension monitoring system with an addition of an RFID readout [15]. The following approach, however, implied a very short communication range. Thus, is only applicable for close up inspection.

Fiber optics sensors [16] gained high traction with various researchers in the recent years using them for different SHM applications, e.g. Zhao et.al. proposed a novel FBG system for SHM [17], a piezopolymer film transducer was proposed by Giannelli *et al*. [18], Hu *et al*. proposed a system to monitor expressway slopes using FBG sensors [19], etc. While these types of sensors do offer some benefits in the form of stability over time, immunity to Electromagnetic Interference (EMI) and ability to measure ultra-fast events, these advantages are only useful for specific use cases. Furthermore, while the size of the sensor itself is small, the subsequent circuitry required to operate it has a significant footprint. This imposes limitations on how compact the end product can be.

From the commercial perspective several companies offer products to monitor the tension of a bolted joint. Notable ones are BoltSafe with its line of continuous logging sensors [20], where a measuring instrument is affixed permanently to the bolt, and periodic logging sensors, in case of which a probe is attached for the reading to be made [21]. Another product manufactured by Industrial Indicators and marketed by the name of SmartBolts uses a visual indicator in a form of a colour changing dot located in the middle of a bolts head to inform about pre-tension level [22]. These approaches, however, are only applicable for close proximity monitoring and require on-site human intervention.

As can be seen most of the proposed designs reviewed are either not suited for remote monitoring completely or offer limited use cases. To solve this problem a solution specified in [23] was developed. However, the preliminary design described was still in immature phase. Thus, the simulation results provided were not accurate enough, battery life estimation did not account for external factors and did not represent the realistic usage scenario, and the communication

coverage was limited to short range. The overall design was still too modular, since the circuitry was split into multiple PCBs. Thus, this paper addresses those issues and presents TenSense M30 – a final iteration of a wireless IoT structural health monitoring node aimed at tracking bolted joints pre-tension load and suitable for use in large structures e.g. bridges, cable clamps, wind turbines, offshore installations, etc.

The objective of this paper is thus to introduce a low cost smart IoT sensor node for the purpose of SHM in a Smart City environment. This addition will allow for a shorter repair response time, since the failure of a joint could be detected and be dealt with before it propagates and causes irreparable damage. This will also lower management costs, since the scheduled maintenance of bolted joints could be made obsolete.

The remaining of the paper is structured as follows:

- Section III describes the specification, design and implementation of three types of TenSense M30 RSHM nodes.
- Section IV evaluates all types of TenSense M30 RSHM nodes in terms of structural integrity, monitoring performance, estimated battery life time, security implementation and transmission range. It then compares the existing solutions to the designed prototypes.
- Section V concludes the paper.

III. TENSENSE: DESIGN OF A PROTOTYPE SENSOR NODE FOR REMOTE STRUCTURAL HEALTH MONITORING

This section introduces the prototype TenSense node and covers its design and evaluation using simulation and experimental tests.

Design of the TenSense node consists of several stages. This includes selection of wireless communication protocol, mechanical design of the washer structure, hardware design, and embedded software design. We have made a Design Specification for our prototype to follow, which is summarized as follows:

- Aim for a miniaturized electronics footprint. Sensing mechanism and components should occupy as little space as possible.
- No physical modifications to the bolt are allowed. Sensing mechanism should be of the non-invasive type.
- No physical modifications to the structure where TenSense node is going to be operational allowed.
- Target for the unattended, remote monitoring with integration into the Smart City ecosystem.
- Use the most efficient communication protocol in terms of coverage and energy consumption.
- Aim for more than 5 year battery life and transmit at least several times per day.
- Ensure the structure of the TenSense node is capable of withstanding the pre-tension load of the fastener.
- Ensure the TenSense node can precisely track the pre-tension load of the bolted joint.
- Ensure secure wireless data transfer.

In order to comply with the above specification most of the steps are either validated by means simulation, practical tests, or backed by extensive research.

A. WIRELESS COMMUNICATION PROTOCOL REVIEW AND SELECTION

A large number of competing wireless communication protocols is available to choose from. This, however, presents a challenge in choosing the right one for the application. To narrow them down to the suitable one we can divide the protocols according to their specified communication range into very short, short and long range ones. Very short communication range protocols are dominated by Radio Frequency Identification (RFID) technology, short ones consist of Bluetooth, Bluetooth Low Energy (BLE), IEEE 802.11x (Wi-Fi), ZigBee, IPv6 over Low Power Wireless Personal Area Network (6LowPAN), etc. The long range communication protocols are divided into cellular and Low-Power Wide Area Network (LPWAN). However, it is necessary to keep in mind that when we are talking about a smart city or any other city, the area that it spans is measured in kilometres. Thus, the use cases for very short and short range protocols will be limited only to certain scenarios discussed below. The latter ones are more suited for implementation in an outdoor environment of a Smart City, as they can cover a larger area, although this also is use case dependent. Table 1 shows the most important characteristics of these protocols and includes a technical overview of modules that support them. This table was constructed with IoT requirements in mind, thus the protocols are examined from this perspective. The majority of the modules supporting the above mentioned protocols can be battery powered. However, the lifetime of the IoT sensor node where the module is installed will mainly depend on the amount of energy stored in the battery and the transmission period. IoT nodes are usually designed to be small, thus they are limited by the space they can provide to accommodate a battery with a larger capacity. Therefore, some careful planning and design trade-offs have to be taken into account. From the table we can see that the most energy efficient modules are the ones that support RFID, Bluetooth 5.0 and 6LoWPAN communication protocols. They are extremely useful in a Smart City environment, however their use case will be only limited to indoor use, since their coverage area is limited compared to modules supporting LPWAN and cellular protocols. Wi-Fi is also better suited for indoor environment, due to majority of the modules supporting it having a significantly higher current consumption and shorter range. Wi-Fi is a feasible option to be used in a base station. Thus, for our application we need to look into long distance protocols.

Both Long Range (LoRa), Sigfox and Random Phase Multiple Access (RPMA) represent the LPWAN. Narrow Band IoT (NB-IoT) is classified as cellular communication protocol and is a step up from Long Term Evolution for Machines (LTE-M) which is targeted at machine-to-machine communication. While clearly cellular protocols offer an excellent coverage due to infrastructure already being in place,

TABLE 1. Communication protocol comparison for IoT applications used in a smart city.

	LoRa	RPMA	Sigfox	NB-IoT	6LoWPAN	Bluetooth 5.0	Wi-Fi	RFID
Frequency	Sub-1 GHz	2.4 GHz	Sub-1 GHz	In-Band LTE	Sub-1 GHz	2.4 GHz	2.4 GHz 5 GHz	LF: 125 - 134 kHz HF: 13.56 MHz UHF: 433 MHz, 860 – 960 MHz SHF: 2.45 GHz 6 -8 GHz
Transmission Current Consumption, mA	47 mA @ 14 dBm	200 mA (min)	65 mA @ 13.5 dBm	255 mA (avg)	22 mA@ 11.6 dBm	9.3 mA @ 5dBm	430 mA	Varies based on the tag type (active or passive)
Receive Current Consumption, mA	21.5 mA	75 mA (min)	25 mA	81 mA (avg)	10 mA	6.3 mA	160 mA	Varies based on the tag type (active or passive)
Power Source for the module	Batteries	Batteries	Batteries	Batteries, Power Supply	Batteries	Batteries	Power Supply	Batteries or Passive
Operational Fees	NA	NA	Per device Per data transmitted	Cellular service fees	NA	NA	NA	NA
Typical Range	up to 15 km	up to 15 km	Rural: up to 50 km Urban: up to 10 km	LTE coverage	110 m	Up to 200m, 40m indoors	~ 50m	LF, HF up to 1m UHF up to 7m SHF up to 90m

All data compiled from datasheets listed in [24]–[30]

the major drawback of modules supporting this technology is the requirement of a SIM card, which inherently translates into additional operational costs, and a larger amount of current consumption during the transmission sequence, which will negatively impact the battery life time in the long run. Thus, LPWAN is a good choice to be implemented in our design. As candidates both Sigfox and RPMA have proprietary stacks and according to the datasheets they consume more current compared to LoRa modules. Furthermore, Sigfox is limited by the amount of messages the device can transmit per day and requires some operational costs [24], [26], [31]. Therefore, LoRa was chosen out of all the LPWAN modules surveyed.

LoRa is a technology developed by Semtech. It represents the Physical Layer (PHY). Long Range Wide Area Network (LoRaWAN) is the Media Access Control (MAC) layer that allows a richer communication subset, e.g. it allows to check the status of the device, change channel, change Spread Factor (SF), etc. by using a set of pre-defined commands. Thus the two should not be confused, as some modules support only LoRa modulation, and do not have the LoRaWAN MAC layer. Compared to other protocols LoRa is partially open sourced. Maximum communication range is specified to be around 15 km, although this depends on the signal path and can be assumed to be applicable only when ideal conditions are met. Some implementations have shown that it is possible to increase the communication distance by making a mesh network, where each LoRa node acts as a relay, as proposed in [32]. The drawback of this implementation is that the sensor node has to be always on. This means that unless the node has a constant power source it will deplete its batteries very quickly. Thus, is not considered for our design.

B. MECHANICAL DESIGN AND IMPLEMENTATION

This step consists of one of the most important parts of the design process – designing a proper washer structure to house the electronics. Since the current TenSense M30 node is aimed at M30 type bolts, hence the naming scheme, it was decided to embed the electronics inside a custom washer and make it a seamless design instead of splitting it into several independent parts like in [33]–[35] where one part houses electronics in a cap, while another is used for tension sensing and both are connected outside by a wire. The chosen approach has several advantages, with the biggest one being integrity. If the node is split into several physical components a high chance of damaging the connection between them exists. A one-piece design eliminates such chance. Therefore it was chosen as the most logical solution. The internal structure of the node was split into several sections, Fig. 2-3. As can be seen the washer has a circular shape, as expected, however the internal structure has 6 hollow sections. The empty space allows for the allocation of hardware components. Three versions were manufactured and they all differ in Z height. This was done to allow the designs to accommodate different sized batteries. The height of the internal hollow section in this case is either 5, 7 or 10 mm. Thus for simplicity this will be referred to as 5, 7 or 10 mm TenSense M30 washer.

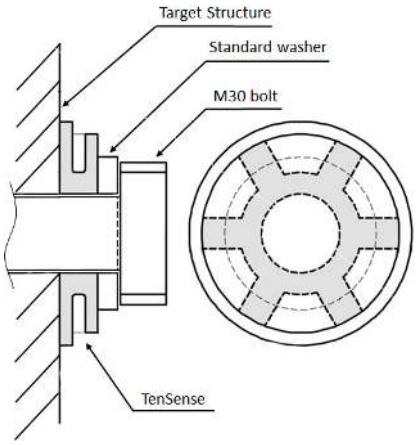

FIGURE 2. TenSense M30 mounting position on a target structure.

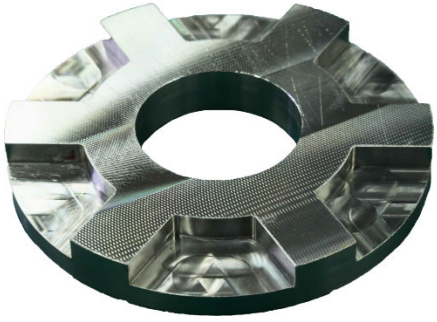

FIGURE 3. Milled One half of the TenSense M30 washer.

To verify the integrity of the washer designs prior to manufacturing we have analyzed their load carrying capacities by means of finite element analysis (FEA). This experiment is needed to ensure that the main function of the designed TenSense M30 washer is not compromised – being a washer. We have investigated the stress propagation in a solid washer (without any cut outs), and all three TenSense M30 washers (with cut outs of different Z height). For this purpose LUSAS software package was used. A wireframe half model was created for each case consisting of two parts - a main washer, represented either by the solid washer, Fig. 4, or a TenSense washer, Fig. 6, and a small Standard washer that usually comes as a part of a set provided with the bolt. This Standard washer is better seen on Fig. 2. Half models were used since we have symmetrical surfaces. A frictional contact with a coefficient of 0.3 was used to connect the standard washer with a TenSense M30 and a pre-tension load of 200 kN was assigned to the top washer in the FEA model. Simulation results are seen in Figs. 5, 7, 8 and 9.

From this simulation we can observe that the stress propagation in a solid washer is uniform, which is an expected result, Fig. 5. The general distribution is below 300 MPa with a number of local stress points of 380 MPa. The simulation results for the 5, 7 and 10 mm TenSense M30 washers show a similar behavior, albeit with a higher degree of stress values.

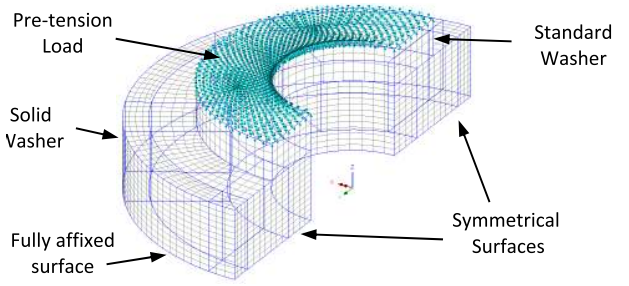

FIGURE 4. Wireframe model of the solid washer with a standard washer.

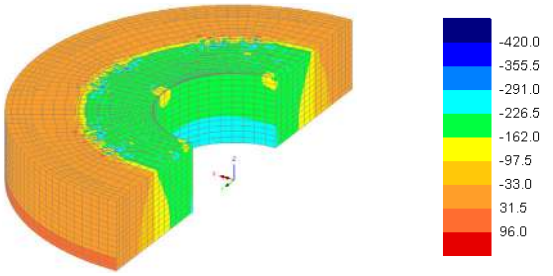

FIGURE 5. Stress distribution in a solid washer.

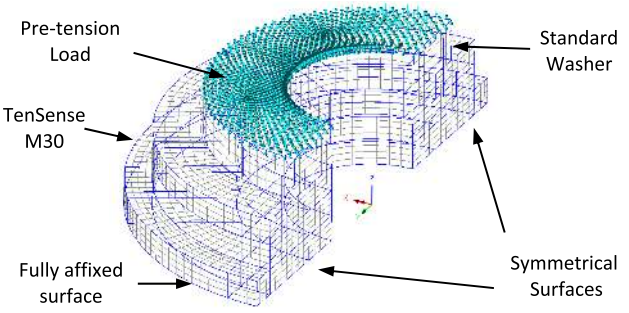

FIGURE 6. Wireframe model of the 5 mm TenSense M30 washer and a standard washer.

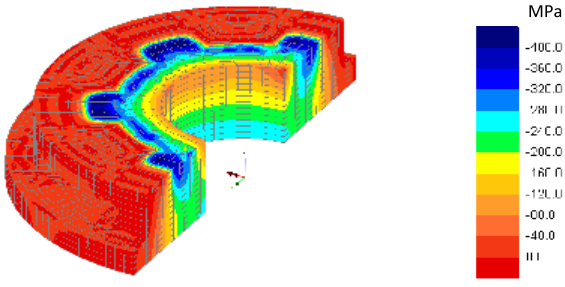

FIGURE 7. Stress distribution in a 5 mm TenSense M30 washer.

The general distribution in all cases is below 400 MPa, Fig. 7-9.

The material used for manufacturing TenSense washer is an austenitic stainless steel. This type was chosen for its corrosion resistance, toughness and fatigue properties. Different grades of this steel exist based on the load bearing capacity. In order for the TenSense washer to be safe under the pre-tension load the stainless material has to have a higher

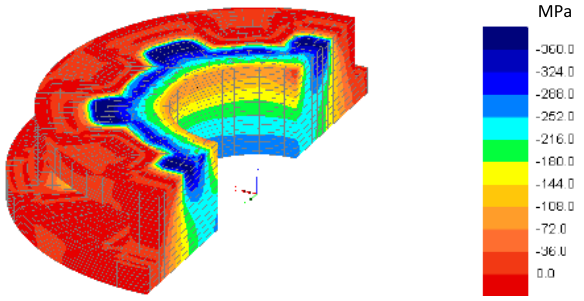

FIGURE 8. Stress distribution in a 7 mm TenSense M30 washer.

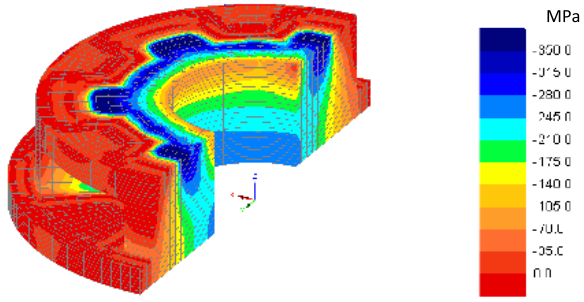

FIGURE 9. Stress distribution in a 10 mm TenSense M30 washer.

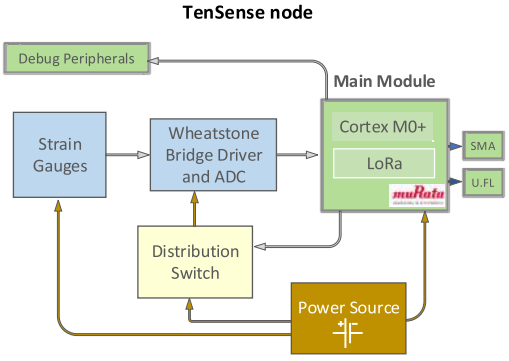

FIGURE 10. TenSense M30 principle top level block diagram.

yield strength than the general stress distribution obtained via simulation. Thus, SUS304N2-X with a yield strength of 450 MPa was chosen.

C. HARDWARE DESIGN AND IMPLEMENTATION

Hardware design consists of the main module, sensing circuitry and conditioning, power management and debug interface. The current design is powered by a number of CR1620 - CR1632 batteries, however the future ones are aimed to include a hybrid between the integrated rechargeable battery and energy harvesting techniques. Fig. 10 shows the top level block diagram of the TenSense node.

The main LoRaWAN module is manufactured by Murata and it was chosen for several reasons. Table 2 provides the summary of the most important LoRa and LoRaWAN module specifications offered by different companies. The main criteria of choice was footprint, current consumption and LoRaWAN MAC layer support for future designs of this project.

As can be seen some modules do not support LoRaWAN, e.g. the ones manufactured by Hope RF and AcSIP, thus they were not considered. Out of the ones that remain, some do not have a host Microcontroller Unit (MCU). This means that an additional one needs to be used for controlling the LoRa module. While this is a good solution for designs that require to use their own MCU, in our case it is important to save space and use an integrated MCU inside the LoRa module. Thus, the module provided by Murata seemed as a good option. Note that the module manufactured by USI comes close to Murata in terms of the footprint, however it lacks proper documentation needed for the design stage, thus is harder to work with.

For strain measurement we have utilized metallic bonded strain gauges as the most practical solution for this kind of application compared to other widely used methods described previously. Strain gauges have been widely used for this type of applications, mainly due to their ability to change electrical resistance in proportion to the amount of strain applied. They have been proven to be accurate if correctly used. As with most of the passive components there are different types of strain gauges. They are manufactured in different shapes and sizes and can have a different resistance. Usually higher resistance is preferred as the effect of self-heating is lower and it helps to account for the lead wire resistance. The latter, however, is not relevant for the current design, as the lead wire length is in the region of 3 cm. There is a possibility, however, that external temperature effects would have an influence on the strain gauges themselves, which could affect the strain reading at different temperature points. This, however, is a known phenomenon and can be compensated for in software by using data from a temperature sensor and apparent stress-temperature profile provided by the manufacturer. Although Cao *et al*. mentioned that despite numerous advantages added to the ones discussed above e.g. cost, ease of manufacture and durability, strain gauges require a complex system to acquire strain information [36], our design proves that this is incorrect. It is possible to minimize the circuitry to a level where the use of bulky loggers is not necessary. In order to get a proper strain measurement from the strain gauges we firstly need to connect them in a specific way. There are several ways to obtain the reading from a strain gauge. The general approach requires a Wheatstone bridge, an excitation source for it, an Operational Amplifier (OpAmp) to amplify the analog signal, a high precision Analog-to-Digital Converter (ADC) to convert it to digital and send it to the MCU. The block diagram for this procedure can be seen in Fig. 11.

Although this is the general way to acquire the data from a strain gauge, we have employed a one chip solution provided by Avia Semiconductor. Their HX711 chip integrates both the Wheatstone bridge driver, Programmable Gain Amplifier, and a 24-bit ADC. Thus, what is left is a correct configuration of the Wheatstone bridge. Depending on a use case, it is

TABLE 2. LoRa and LoRaWAN module comparison.

	Microchip RN2903	USI	Murata CMWX1ZZ ABZ-078	HOPE RF RFM95	MIPOT 32001409	Miromico FMLR (STM)	AcSIP CW1276SL-915	GlobalSat LM-130H1
TX Current Consumption	124 mA @ 18.5 dBm	127 mA @ 18.8 dBm	128 mA @ 20 dBm	120 mA @ 20 dBm	70 mA @ 10 dBm	125 mA @ 20 dBm	Not Specified	125 mA
Host MCU	None Control via UART	STM32L052 ARM Cortex-M0+	STM32L082 ARM Cortex-M0+	None Control via SPI	None Control via UART	STM32L151 ARM Cortex-M3	None Control via SPI	STM32L151 ARM Cortex-M3
Radio Transceiver	RN2903	SX1272	SX1276	RFM95	SX1272	SX1272	SX1276	SX1276
LoRaWAN Class	A	A and C	A and C	-	A and C	A	-	A
Form Factor	17.8 x 26.7 x 3.34 mm	12.0 x 13.0 x 2.0 mm	12.5 x 11.6 x 1.76 mm	16 x 16 x 1.8 mm	15.5 x 26 x 3.16 mm	14.0 x 22.0 mm	16 x 16 x 1.75 mm	25 x 18 mm

Module data is compiled from [24], [37]–[43] datasheets

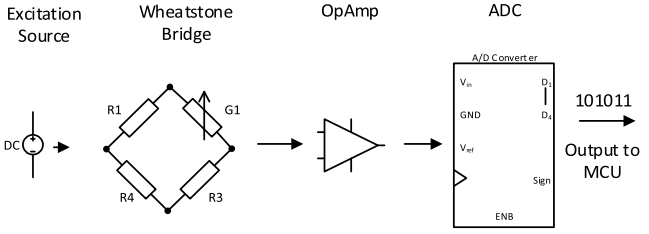

FIGURE 11. Electronic circuit block diagram for reading the strain gauges.

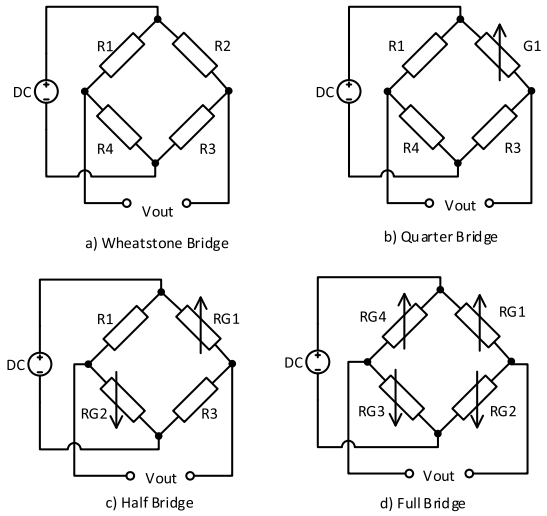

FIGURE 12. Wheatstone bridge configurations.

possible to use one, two or four strain gauge configuration, Fig. 12. Quarter bridge or half bridge is usually used, with the full bridge being the most sensitive one to the strain change, although this also depends on the strain gauge placement. It is possible to have some gauges configured as dummies and use them for temperature effect compensation. In this design half bridge configuration is used and the HX711 chip is capable of driving two Wheatstone bridges, meaning

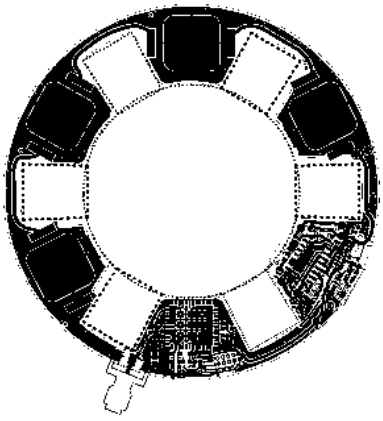

FIGURE 13. TenSense M30 PCB layout.

we can monitor the strain change in two different washer locations.

We have utilized a TI TPS2065 high side switch to power gate the HX711 ADC. Since there is no necessity for it to be operational all of the time. Even putting it to sleep mode would contribute to gradual battery depletion, thus disconnecting it from the power rail completely when it is not in use is a perfect solution to prolong battery life.

TenSense PCB layout can be seen in Fig. 13 with an assembled design pictured in Fig. 14. For testing purposes PCB is equipped with numerous debug points and indicators that enable us to verify the correct operation of the design. It also has several headers for the antenna, full sized SMA and UF.L for using a custom designed antenna. Naturally only one can be used at the same time, since leaving both of them at the same time connected to the antenna signal output pin of the LoRaWAN module would have a negative impact on the performance of the connected antenna. The path is selected by installing or removing a 0 Ohm resistor.

As can be seen from the figure above out of the six sections four can be occupied by the coin cell batteries connected in

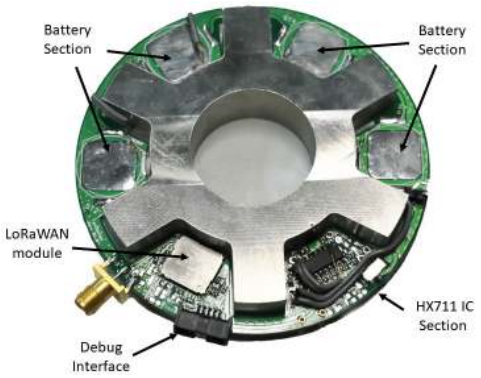

FIGURE 14. Assembled and mounted PCB for experiments.

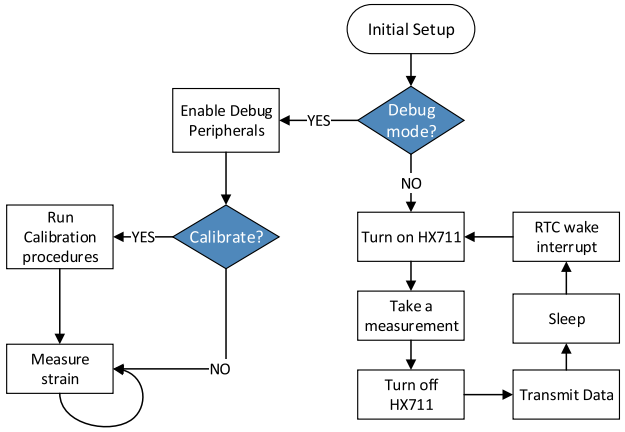

FIGURE 15. Software flowchart.

parallel and out of the remaining two sections one is dedicated to the LoRaWAN module and the other one for the HX711 IC.

D. SOFTWARE DESIGN

Currently the embedded software allows the TenSense node to function in a debug and peer-to-peer (P2P) communication modes. Debug mode allows to fully monitor the steps performed by the node via onboard LEDs and wired USART communication allowing to check for the correctness of the software execution. Debugging peripherals are not needed when the node is configured in a P2P mode, thus are disabled. Simple block diagram is provided below and as can be seen the operation of the node is quite straightforward.

E. SECURITY IMPLEMENTATION IN A LoRa COMMUNICATION CHANNEL

LoRaWAN, as an additional MAC layer for LoRa technology, introduced a richer communication subset. The protocol is optimized towards low cost, energy efficiency and security. However, Yang *et al*. proved that LoRaWAN is vulnerable numerous attacks e.g. replay, eavesdropping, bit-flipping, ACK spoofing, and LoRa Class B attacks [44]. In addition to that, LoRaWAN is rarely used for industrial applications where implementation of a private network is more desirable.

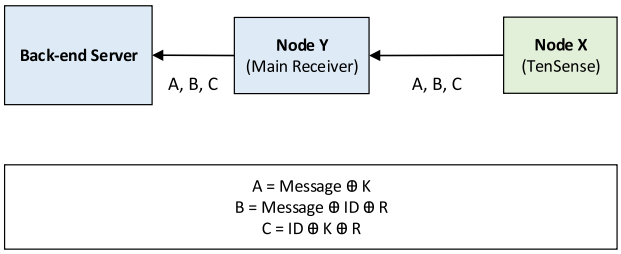

FIGURE 16. Proposed LoRa P2P communication protocol.

This is mainly due to several limitations, which include interference introduced by several LoRaWAN networks trying to co-exist in the same area at the same time, high packet error rate, no guarantee of receiving the message, complex development work due to involvement of different parties, etc. Therefore, a simple P2P LoRa communication that allows a direct long distance link between the nodes was chosen for this project. Unlike LoRaWAN, LoRa P2P communication does not have any security features that can be used to ensure data integrity during the transmission sequence. Therefore, it is important to ensure that the data sent to a peer node is secure from a number of attacks that include replay, tracking, and man-in-the-middle attacks. Hence, instead of sending a message in a plaintext format, it should be encrypted before transmitting it to the peer node. Since TenSense M30 is a resource constrained device due to a low power MCU utilized in the module, it is only able to support lightweight cryptographic algorithms, such as bitwise exclusive-or operation.

A basic LoRa P2P communication involves three parties, which include the peer nodes (Node X, acting as the TenSense M30 node, and Node Y acting as the main receiver) as well as back-end server for storing the received data. An assumption is made where the communication channel between the Node Y and back-end server is secure, whereas the communication channel between the peer nodes is insecure.

For this protocol to function during the initial phase Node X needs to store two pieces of secret data: *ID* and a private key, *K*. In contrast, the back-end server stores three pieces of secret data: *ID*, *K*, and a timestamp. Each node is identified by its unique *ID*, with the corresponding private key *K*. The function of the Node Y or main receiver is to receive messages sent from Node X, TenSense M30, and then forward it to the back-end server. Messages sent from the TenSense M30 to the main receiver are comprised of a concatenation of a timestamp and the strain value collected by the TenSense.

The communication process of a LoRa P2P system shown in Fig. 16 is described as follows:

1. After the strain value is measured by TenSense M30, the Node X generates a random number, *R*, it then computes and transmits strings *A*, *B*, and *C* to the main receiver Node Y.
2. After receiving the strings, Node Y forwards the strings *A*, *B*, *C* to the back-end server.

3. The back-end server extracts R' from string C, by using the stored (ID and K) pair values, and performs the operation until matched strings A and B are obtained using the stored (ID and K) pair and the extracted R' value.
4. The back-end server then extracts the Message from strings A and B. If the Message is equal, then back-end server extracts the timestamp and the strain value from the Message.
5. The back-end server verifies the extracted timestamp and the stored timestamp. If the extracted timestamp is equal or earlier than the stored timestamp, the communication session ends. Otherwise, the back-end server updates the current Message according to the ID and K pair in its database.

IV. EVALUATION AND DISCUSSION

The design evaluation part consists of a number of tests that help to evaluate the performance of TenSense M30 nodes.

These are as follows:

- Compression test. Physically evaluates the structural integrity of the TenSense washers to ensure they are safe under the pre-tension load.
- Strain measurement performance. Shows how precise TenSense M30 nodes can measure the strain compared to the Reference Logger and the simulation data.
- Current consumption using pre-defined scenarios.
- Transmission distance in P2P mode. Evaluates the coverage.
- Security evaluation of the proposed LoRa P2P communication protocol and comparison to LoRaWAN.
- Feasibility study and challenges of using small coin cell batteries in this design.
- TenSense M30 comparison to other designs.

A. COMPRESSION TEST

This test was performed in a controlled environment with the setup pictured in Fig. 17.

A 5 mm TenSense M30 washer was equipped with a number of Tokyo Measuring Instruments Labs (TML) FLA-05-11-1LJC 120R strain gauges each having a 120 Ohm resistance. 7 mm and 10 mm TenSense washers used TML FLA-3-11-1LJC 120R and FLA-5-11-1LJC 120R strain gauges respectively. Tokyo Sokki Kenkyujo CN-Y cyanoacrylate adhesive was used to affix them inside the structure of a TenSense M30 washer. It is possible to mount the strain gauges either longitudinally or transverse. However, the amount of strain measured will be different in both cases, with the former providing higher value. Thus, longitudinal mounting is used for all TenSense M30 washers. Placement of the strain gauges inside the prototype can be seen in Fig. 18. A pair of gauges was used for strain measurement by the TenSense M30 node itself, and another pair was used by the reference Tokyo Measuring Instruments Lab TDS-530 data logger.

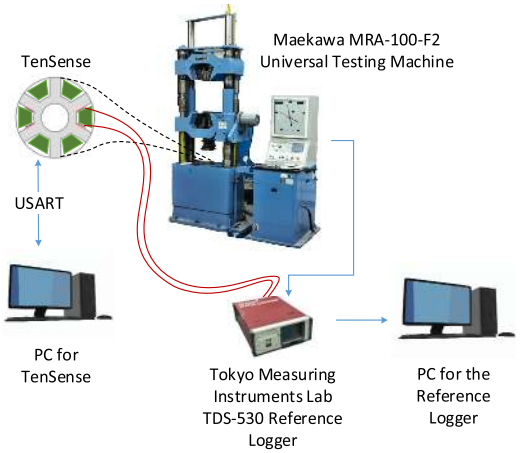

FIGURE 17. Experimental setup.

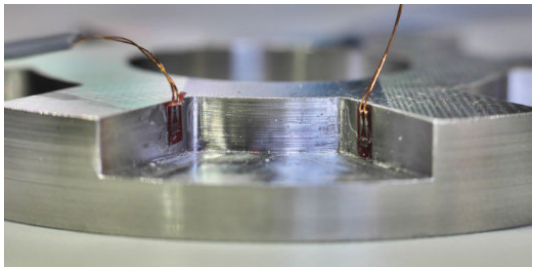

FIGURE 18. Strain gauge placement for 5 and 7 mm TenSense M30.

A Maekawa MRA-100-F2 Universal Testing Machine was used to apply the force to the TenSense M30 washers. This force was in the range of 0 to 400 kN. Although the machine is capable of applying a greater force of up to 1000 kN, the chosen range is sufficient to test both the performance of the TenSense M30 node and the structural integrity of the washer, since the pre-tension load in a real world applications for M30 type bolt is in the region of 400 kN.

In order to obtain a meaningful data from any TenSense M30 node, firstly, it had to be calibrated. This procedure is split into two steps – nulling and setting the calibration factor. Nulling, as the name states, is counting the current output value of the Wheatstone bridge as 0. Due to component tolerances there is always voltage at the output of the Wheatstone bridge, even when the strain gauges are not stressed. Thus, this needs to be accounted for and will serve as a correct starting point for consecutive measurements. This procedure is done when no load is applied to the TenSense washer. Once done a calibration factor needs to be set. Calibration factor is used to return the data in understandable format and is done by applying a known load to the TenSense washer. Calibration factor is set once, while nulling, for the purpose of the experiment, can be done every time. Firstly, TenSense node was calibrated by applying a 200 kN force to it, which corresponded to -850 microstrain based on the reference logger. Note that negative strain values correspond to compression, positive correspond to tension. After this

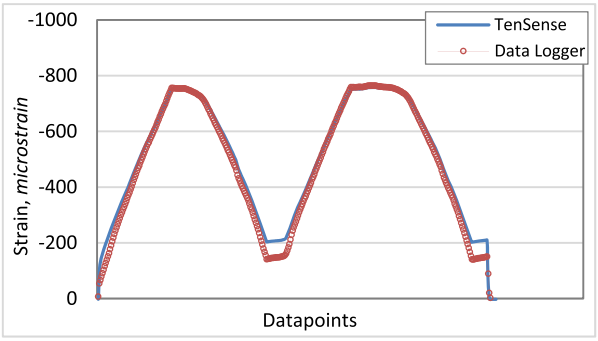

FIGURE 19. Experimental profile results for 5 mm TenSense M30 node.

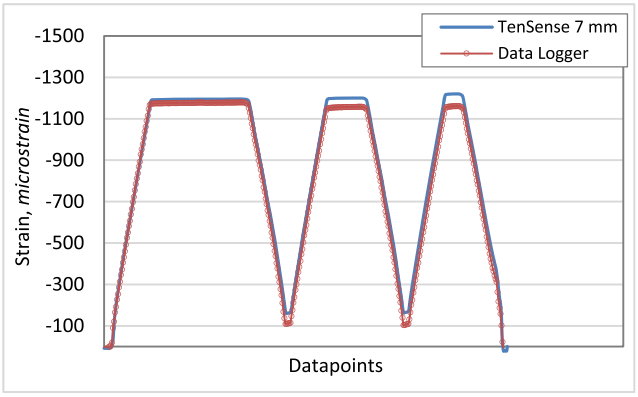

FIGURE 20. Experimental profile results for 7 mm TenSense M30 node.

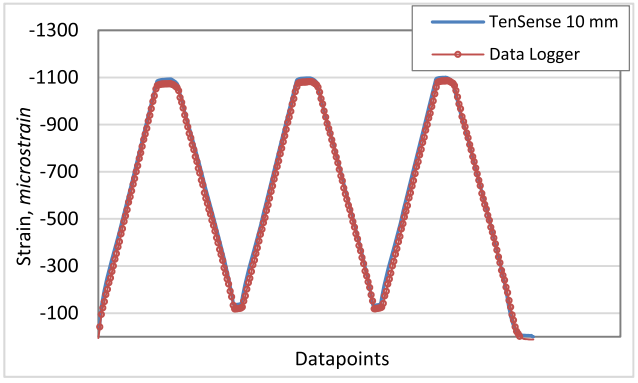

FIGURE 21. Experimental profile results for 10 mm TenSense M30 node.

procedure the TenSense M30 node was ready to measure the strain. We have made a pre-defined measurement profile for the compression machine which consisted of gradually applying a force to TenSense node from 0 kN to 360 kN level, holding the load for a period of time and then decreasing it to 100 kN. The process was then repeated by increasing the load to 360 kN and decreasing to 100 kN, followed by fully de-loading the sample. The following graphs visualize the data obtained from the TenSense node and the reference data logger, Fig. 19. There is a slight difference between the gathered data, which can be explained by the nature of the experiment, since both the data logger and TenSense M30 node are using gauges that are placed on opposite sides of the washer. Thus, while the gauges themselves are of the same type, their placement on the structure of the washer is not exactly perfect.

Using a strain gauge with a larger active area logically would provide better response. However, the 5 mm TenSense is restricted on available space. The duration of the experiment is irrelevant in this case, since we are only interested in the response of the designed system compared to the reference logger. While there is a slight difference in the lower region, the upper shows identical behavior. Similarly the calibration procedures and experiments were conducted for 7 and 10 mm TenSense M30 nodes respectively, albeit using slightly different measurement profiles, Figs 20-21. The maximum loading during experiments for 7 and 10 mm TenSense nodes was 400 kN. Furthermore, the placement of the strain gauges for 10 mm washer is different compared to 5 and 7 mm washers.

The strain value at the inside wall of the TenSense node is lower compared to the center. Thus, in order for the 10 mm TenSense node to better sense the strain the gauges were placed at the center wall.

According to the theory strain values should increase linearly with respect to the applied force. To confirm this behavior we have simulated the stress propagation in TenSense washers under different loading conditions. The following figures show the stress propagation at 100, 195, 290 and 400 kN of force applied to the structure in a 5 mm washer, Fig. 22 a–d respectively. We can see that the stress propagation in the area where strain gauges are placed is not fully

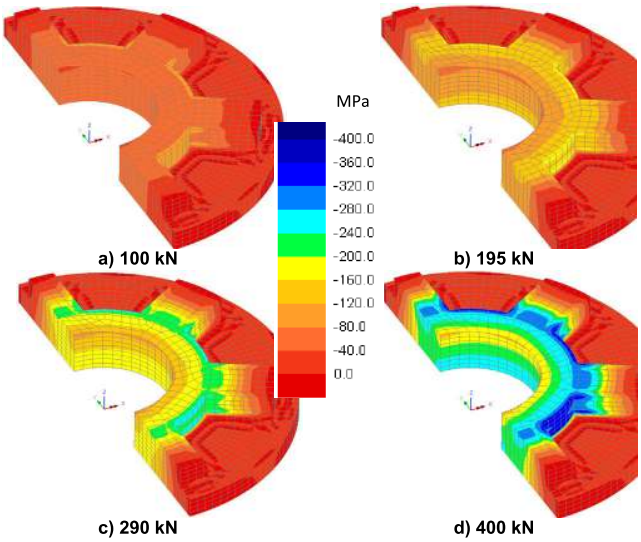

FIGURE 22. a-d. Stress propagation under different loading in a 5mm TenSense M30 washer.

uniform. A better example can be seen in Fig. 23 a-d where the black rectangles denote the strain gauge placement.

This non uniformity would also explain the difference in experimental results obtained during the previous experiment. Since a slight placement variation would directly affect

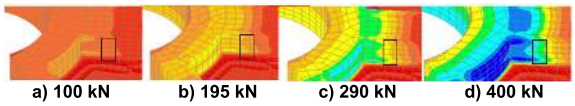

FIGURE 23. a-d. Strain gauge placement and corresponding stress propagation in the local area under different loading conditions.

the obtained strain value. 7 mm TenSense washer has the same placement and exhibits a similar trend. Nonetheless, the vital part is the linear correlation between strain and the load. To confirm this behavior a number of strain values were taken from the FEA simulation models for 5, 7 and 10 mm TenSense M30 washers at the point where the strain gauges are supposed to be mounted. These values were then plotted against the force applied to the washer, Fig. 24. This was then compared to the experimental data obtained from the previous experiments for all 3 TenSense M30 washers. Plotting the experimental data on the same graph reveals a similar behavior. Although there is a discrepancy in the lower region, specifically below 50 kN, it can be explained by the conditions of the experiment and lower accuracy of the compression machine when a small amount of force is applied to the sample. Both the Data Logger and TenSense show the same trend. The region of interest and the area where it is vital to monitor the tension values is in the upper band, where the pre-tension force is in the region of 350-400 kN. For different TenSense washers this corresponds to a different strain value, since strain value depends on the area of propagation. This means that a 5 mm TenSense washer will have a higher stress value over the same area, compared to 7 and 10 mm ones. This can be clearly seen from the experimental profiles, Fig. 19 - 21 and 24. This experiment proves that TenSense M30 is fully capable of precisely monitoring the tension of a bolted joint in the area of interest. However, just monitoring is not enough. In order to know when the bolt needs to be re-fastened logically we need to set a threshold that would signal to dispatch maintenance. By requirement the recommended pre-tension force for the M30 bolt should be in the region of 379 kN going up to 417 kN. The safety factor in this case is 10 %. Thus, our threshold can be set just below 379 kN. Different TenSense M30 nodes would have a different strain value at that pre-tension load, which is an easily obtainable value.

B. CURRENT CONSUMPTION ESTIMATION

This part looks into the current consumption of the TenSense M30 node during its operational mode. A reference table is made consisting of current consumption numbers for different transmission power modes compiled from the datasheets, Table 3. These numbers, particularly current consumption during transmission sequence at different power level, were then compared to the experimental ones obtained by using the GWInstek GDS-310 oscilloscope paired with an AIM TTi I-prober current probe. Results are visualized in Fig. 25. Based on it we can clearly observe variation between quoted

TABLE 3. Current consumption of TenSense M30 based on the datasheet values.

Current Draw Mode	Murata Module STM32L082 MCU	Murata Module SX1276 IC	HX711
On Mode	3.2 mA @ 16 MHz	1.6 mA	1.5 mA
Sleep Mode	0.86 uA	0.2 uA	0 uA (power gated)
Transmission Mode	128 mA @ 20 dBm 106 mA @ 17 dBm 47 mA @ 14 dBm 34 mA @ 7 dBm		

numbers and experimentally obtained ones. The largest difference being when the low power transmission mode is chosen, where in reality the module requires more current to transmit. Thus, for the purpose of calculating the yearly current consumption and needed budget experimental values were used. Although the 20 dBm power mode might seems high, since the current consumption is in the area of 121 mA, the time-on-air, i.e. amount of time it takes for the module to transmit the packet, is very short.

In our case it is 10 ms. This duration is dependent on a Spread Factor (SF) setting used for LoRa communication. The bigger SF increases time-on-air. Thus, the current consumption will mainly depend on the transmission period and current consumed during the sleep time. Fig. 26 shows the current required to power the node throughout the year. The calculations were made based on the following assumptions: time-on-air is 10 ms, time required to take the measurement is 1 s, and remainder of the time is allocated for sleep mode. Keeping in mind the 3 modes specified in Table 3, to calculate the average hourly current draw we need to sum up the currents used during all those modes. Assuming we only transmit once, then during On Mode, when the measurement is being taken by HX711 IC and the STM32 chip is doing the calculations the current consumption is equal to 0.00175 mA. During Sleep Mode the consumption is 0.00106 mA per hour. During Transmission Mode the consumption is dependent on the power mode used, which is either 0.00035 mA, 0.00027 mA, 0.00018 mA or 0.000138 mA for 20 dBm, 17 dBm, 14 dBm and 7 dBm power modes respectively. Based on the assumptions, there is little difference in yearly current consumption between the modes, as can be seen from the Fig. 26, provided the number of transmission times is kept below 25. Thus using the highest transmission power mode of 20 dBm will not impact the battery life dramatically in this case.

C. FEASIBILITY INVESTIGATION OF POWERING THE DESIGN WITH A SMALL COIN CELL BATTERIES AND BUDGET REQUIREMENT

Most of the modules used for communication in IoT devices are targeted to be battery powered. However, we can claim

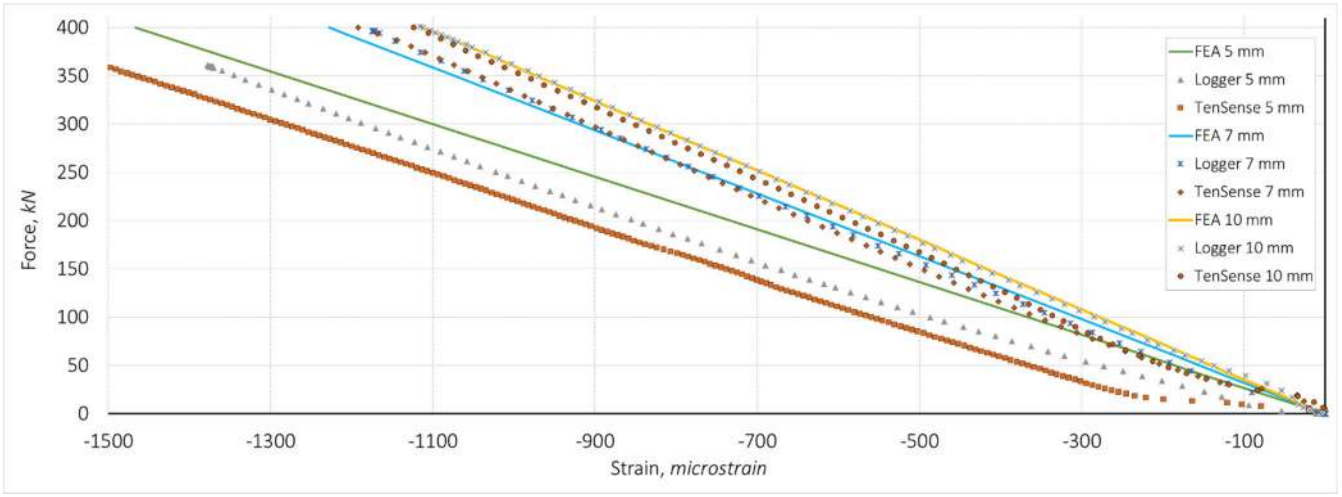

FIGURE 24. Strain and force correlation in a 5, 7 and 10 mm TenSense M30 washers compared to the simulation results (FEA, represented by solid lines) and results obtained by the reference logger.

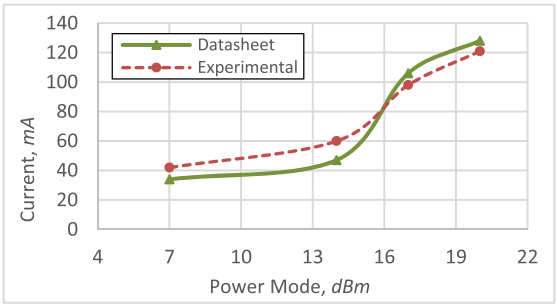

FIGURE 25. Current consumption during power transmission mode.

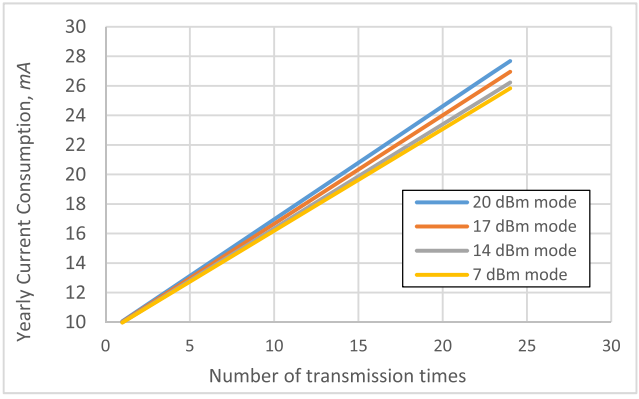

FIGURE 26. Yearly current consumption dependency on transmission power mode.

that "battery powered" part is very vague due to the fact that there are various batteries that utilize different chemical elements to convert the chemical reaction into electricity. The end result is a broad range of batteries with various shapes and sizes capable of storing and providing a limited amount of energy for a certain amount of time. Since there are different current requirements for different IoT modules, i.e.

TABLE 4. 16mm coin cell battery specification.

Battery Type	Nominal Voltage, V	Typical Capacity, mAh	Discharge Current, mA	Pulsed Discharge Current, mA
CR1616	3	50 - 70	0.06 - 0.1	4 - 6.6
CR1620		80 - 95	0.06 - 0.1	4 - 8
CR1625		95 - 110	0.06 - 0.1	4 - 15
CR1632		120 - 150	0.08 - 0.1	4 - 30

powering a LoRa module is not the same as powering a Bluetooth module, not all batteries can be used for this purpose. Thus the feasibility of using small coin cell batteries in the design needs to be examined. 16 mm coin cell batteries are the candidates. They are separated based on their thickness into different types, namely CR1616, CR1620, CR1625 and CR1632, although different manufacturers can add various prefixes instead of CR in case the battery requires special mounting or utilizes advanced chemistry.

The most important characteristics of the battery in our case are the capacity and discharge current. Typical capacity is based on the end voltage of the battery, which is 2V, and there are various factors that affect it. Two major ones are the operating temperature and discharge rate. Operating the batteries under normal manufacturer advised conditions will yield the actual capacity close to the advertised one. However, operating outside of them will have an adverse effect, e.g. pulsed drain can decrease the capacity by 20-50% [42]–[46]. Since TenSense M30 node sleeps most of the time and requires a large amount of current only when it transmits, this sequence will be considered as a pulsed load. Pulsed discharge current is battery dependent, with the average value being 12 mA for CR1632 battery. Murata, however, offers batteries capable of providing 30 mA of pulsed current

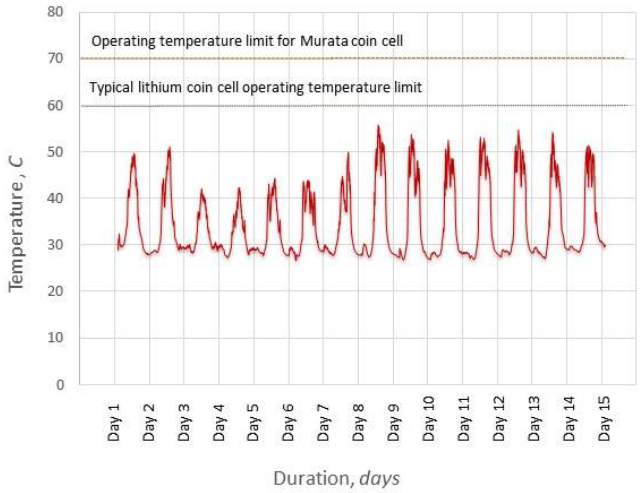

FIGURE 27. Surface temperature of the TenSense M30 node.

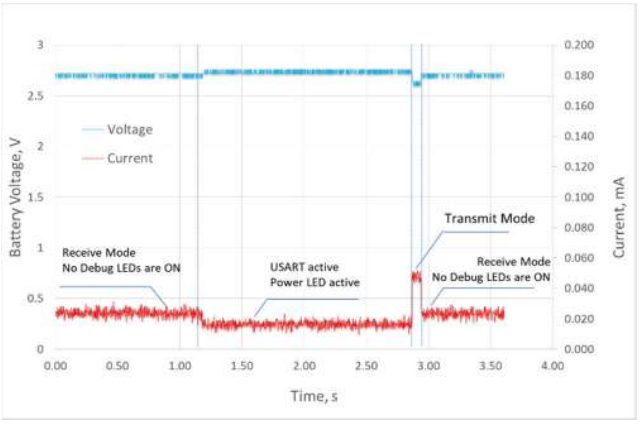

FIGURE 28. Active current vs. battery voltage during operational mode.

according to [47]. Temperature is another factor that degrades battery life, sub 0°C conditions have a more pronounced effect on the capacity and the open circuit voltage, where both of these parameters degrade severely. While temperatures close to 60°C increase the open circuit voltage, for some types of batteries these operating conditions are undesirable. A field test has been carried out to confirm the surface temperature of the TenSense node during the peak summer season in Japan when temperature rises to its extreme level. Logging commenced in the beginning of August. TenSense node was placed under direct sunlight and its surface temperature was monitored throughout the period of several weeks, Fig. 27.

It is clearly visible that the node can easily heat up beyond 50°C degrees peaking at 55 °C during daytime and it is safe to assume that higher temperatures are also possible. Most of the standard lithium coin cell batteries can safely operate in an environment of up to 60°C. Thus it is not advisable to use them as they would be operating close to their limits. This is mostly due to the liquid electrolyte used. The above mentioned Murata CR1632 battery can tolerate temperatures of up to 70°C, thus can be considered as a candidate. However, batteries with advanced chemistry are also available. Manufacturers claim they are able to operate in harsh environments of up to 110°C, thus present a better choice for our application to mitigate the effects of high temperature.

We have further examined the pulsed load effect on the battery voltage in our prototype. Fig. 28 shows the current consumption of the TenSense M30 node and the voltage of the supply rail.

7 dBm transmission power mode was set for this experiment and 4 CR1620 batteries were used. During the transmission sequence, as expected due to the higher load, the supply voltage momentarily drops and then recovers, since a larger current demand was introduced. There are several solutions to this problem. One is to use a larger number of batteries connected in parallel. This inherently would lead to a better load handling. However, this approach is not always applicable since space restrictions apply. Thus, alternative solution would be to use a supercapacitor as a bulk storage. In this case the supercapacitor would partially take the load off the batteries during the peak current demand. In our design the 10 mm TenSense node can accommodate 10 CR1632 batteries. This is done by stacking an additional PCB that houses more batteries. The total theoretical capacity under normal operating conditions in case of using the 130 mAh batteries sums up to be 1300 mAh. However, taking into account the use case scenario and all the factors listed above that affect the performance of the battery, for the current application their efficiency for 10 mm TenSense M30 node was assumed to be 60%. Thus, this lowers the available capacity to 780 mAh. In case of 7 mm and 5 mm TenSense M30 nodes the amount of batteries they can accommodate is lower and equal to 4 since there is no space to include an additional PCB. These batteries theoretically will experience a heavier effect of high current drain during transmission sequence, even with using a supercapacitor, thus it is safe to assume the efficiency will drop to 55%. The available capacity is then 286 mAh for 7 mm TenSense using CR1632 batteries and 187 mAh for 5 mm TenSense paired with CR1620 batteries. According to Fig. 26, in the worst case scenario the transmission period for 5 mm TenSense should be restricted in order to achieve a larger than 5 year lifetime target by using the 20 dBm power mode.

D. TRANSMISSION COVERAGE

There are numerous factors that affect the transmission distance. On the hardware side these are the characteristics of an antenna used on both ends – receiver and transmitter. Other important factor is the transmission power mode selectable both by the transmitting and the receiving modules. Finally, the placement of the receiver antenna plays a great role. Typically it has to be placed where no or little obstructions are in sight. The part that we cannot control is the environment, i.e. the path taken by the signal from transmitter to receiver. As the signal propagates on its way it may encounter

FIGURE 29. Signal transmission path. Google earth image overlay.

obstacles such as buildings, trees, etc. which will reflect, scatter or reduce its strength inherently affecting the distance it can travel. For this experiment we have set up the TenSense M30 in P2P mode and enabled the +20 dBm power mode. The STM32L0 Discovery LoRa development board acted as a base receiver and the power setting was set to +20 dBm. The location of the base receiver was indoors to represent the non-line-of-sight scenario. With this setup the maximum transmission distance was recorded to be around 800 m, Fig. 29. Beyond this distance the communication became erratic. LoRa has a poor building penetration, thus the indoor placement of the base receiver degraded the transmission performance severely. For future experiments we will utilize a typical outdoor placement of the antenna for the base receiver to evaluate the line-of-sight transmission distance. Furthermore, there is a possibility to increase the transmission distance in the current setup by setting a higher SF, which is software selectable in the range from 6 to 12. This approach would result in a longer time-on-air, since a higher SF by design requires a longer time to transmit the same amount of data, thus impacting the battery lifetime.

E. SECURITY ANALYSIS OF THE PROPOSED P2P LoRa COMMUNICATION CHANNEL

The safety of the proposed LoRa P2P communication sequence was analyzed against five following attacks.

1) TRACKING ATTACK

The identity of Node X can be verified by using the secret data *ID* and K. Since this data is encrypted either by a Message consisting of a new timestamp (string A), or a new random number, R (string C), or using both the Message and random number (string B), there is no constant response sent by the Node X that can be used by the attacker for tracking purposes.

2) MAN-IN-THE-MIDDLE ATTACK

Attacker is unable to modify Message sent from Node X to the Node Y because the data integrity of a Message can be guaranteed by strings A and B. Since the attacker is unable to guess the values of secret data, *ID* and K, it is impossible for him to modify Message in both strings A and B encrypted with different secret data.

3) REPLAY ATTACK

Attacker is unable to replay strings A, B, and C to the Node Y, because the replayed strings can be detected by comparing the stored timestamp and the extracted timestamp from Messages in string A and B.

4) KEY DISCLOSURE ATTACK

Private key K is encrypted with a new random number R for each new session in a string C. In addition,K in a string A is encrypted with a Message that is concatenated with a new timestamp and a strain value for each new session. Therefore, it is impossible for the attacker to guess the values of K based on the strings A and C.

5) DE-SYNCHRONIZATION ATTACK

Since the secret data is not updated in each new session, there is no de-synchronization issue with the secret data between Node X and the back-end server.

F. PROPOSED P2P LORA COMMUNICATION PROTOCOL COMPARISON TO LoRaWAN

The proposed protocol was then compared with a LoRaWAN protocol in terms of security features and performance, Table 5. As can be seen, the proposed protocol is not only able to protect the LoRa system from all 5 attacks, but it also outperforms the LoRaWAN protocol in terms of lower storage, and both computational and communication costs. The proposed protocol requires an end device to store 128 bits of K and *IDS*, where the total storage cost is merely 256 bits. In contrast, LoRaWAN protocol requires an end device to store 640 bits of data before the activation process takes place. This process is required for the device to initially join the LoRaWAN network and is referred to as Join Procedure. After the process is successful additional 544 bits of session data is stored. The total storage cost of a LoRaWAN protocol is thus 1184 bits.

Let T_{xor} and T_{AES} denote the time needed for executing an exclusive-OR and AES operations respectively. The proposed protocol requires a computational cost of 5 T_{xor}, whereas LoRaWAN requires a computational cost of 10 T_{AES} and 10 T_{xor}. Wu *et al*. deduced that the computational cost of an exclusive-OR operation, T_{xor} can be ignored since this cost is substantially lower compared to T_{AES}, which requires 0.0056 s [48].

The proposed protocol transmits 3 strings (A, B, C) to the peer node, and each string is 128 bit long. Therefore, the total communication cost is merely the cost of transmitting 384 bits, whereas LoRaWAN protocol requires at least 520 bits for Join Procedure, without including the communication cost for uplink and downlink messages.

G. TenSense M30 COMPARISON TO AVAILABLE SOLUTIONS

According to the specifications outlined in the beginning of the paper the design fully achieves all of the set goals. Table 6 summarizes the advantages of the TenSense M30 compared to the existing proposed designs.

TABLE 5. Proposed protocol comparison to LoRaWAN.

Description	Proposed Protocol	LoRaWAN	LoRa
Unique Identifier	128 bit ID	64 bit DevEUI	Undefined
Encryption type	Symmetric	Symmetric	NA
Encryption algorithm	Exclusive-OR	128-bit Advanced encryption standard (AES) Exclusive-OR	NA
Secret key	128-bit private key, K	128-bit Application key (Appkey) 128-bit Network key (NwkKey)	NA
Storage cost at end device (bit)	256 bits	1184 bits	Undefined
Computational cost (seconds)	5 T_{xor}	10 T_{AES} 10 T_{xor}	NA
Communication cost (bits)	384 bits	520-bit for OTAA join procedure Unknown bit for uplink and downlink message	Undefined
Resistance to tracking attack	YES	YES	No
Resistance to replay attack	YES	No	No
Resistance to man-in-the-middle attack	YES	No	No
Resistance to key disclosure attack	YES	No	No
Resistance to de-synchronization attack	YES	No	No

TABLE 6. TenSense comparison to current solutions.

Solution	Wireless Data Logging	Requires External Circuitry	Requires Bolt Modifications
TenSense M30	Yes	No	No
SmartBolts	No	No	Yes
BoltSafe	No	Yes	No
FBG Based System	No	Yes	Yes
PZT Based System	No	Yes	No

As can be seen the proposed TenSense M30 node allows to log the data remotely, requires no additional equipment at the target structure and requires no modifications to the bolt itself or the target structure. Wireless data logging is a vital feature for SHM and should not be underestimated. Based on the collected data it allows to predict and mitigate a fault in bolted joints before irreversible damage happens. Other systems can be adapted for remote logging, however they would require external circuitry, in case of BoltSafe, FBG and PZT based systems. SmartBolts can be adapted for remote logging by including a color readout sensor positioned at the center of the bolt. Thus, at this stage, TenSense M30 can be counted as the ideal solution for remote bolted joint monitoring.

V. CONCLUSION

This paper presented a novel bolted joint pre-tension monitoring IoT sensor node – TenSense M30, aimed for integration into the smart city environment. Compared to the existing solutions on the market the proposed design allows for remote precision monitoring of a bolted joints pre-tension load without any modifications required to the target structure or the bolt itself. Both FEA analysis and physical evaluation of the TenSense M30 node proved the design is safe under the applied pre-tension force. Furthermore, the physical tests clearly showed that the system is capable of precisely tracking the corresponding strain. The proposed communication protocol ensures a secure channel via LoRa P2P. Thus the link is safe against common attacks, e.g. tracking, man-in-the middle, de-synchronization, replay and key disclosure ones. Battery life is estimated to be longer than 5 years in a worst case scenario when the 20 dBm transmission mode is used. Current coverage range extends to more than 800 m in a non-line of sight scenario. All of this ensures that the design is fully capable of tracking the health of the target construction on a daily basis.

The current project will further be expanded to include the possibility of monitoring the pre-tension load of smaller sized bolts, e.g. M20, M22, M24 and M27. Furthermore, the effect of using different spread factors for LoRa communication and its effect on transmission distance and power consumption will be investigated in the current and future designs.

ACKNOWLEDGMENT

This project is done in collaboration with our industrial partner Toyo Metal Co., Ltd., and the authors would like to thank them for their continuous support.

REFERENCES

[1] S. P. Mohanty, U. Choppali, and E. Kougianos, "Everything you wanted to know about smart cities: The Internet of Things is the backbone," *IEEE Consum. Electron. Mag.*, vol. 5, no. 3, pp. 60–70, Jul. 2016.

[2] P. M. Santos, J. G. P. Rodrigues, S. B. Cruz, T. Lourenço, P. M. d'Orey, Y. Luis, C. Rocha, S. Sousa, S. Crisóstomo, C. Queirós, S. Sargento, A. Aguiar, and J. Barros, "PortoLivingLab: An IoT-based sensing platform for smart cities," *IEEE Internet Things J.*, vol. 5, no. 2, pp. 523–532, Apr. 2018.

[3] A. Zanella, N. Bui, A. Castellani, L. Vangelista, and M. Zorzi, "Internet of Things for smart cities," *IEEE Internet Things J.*, vol. 1, no. 1, pp. 22–32, Feb. 2014.

[4] J. M. Schleicher, M. Vögler, S. Dustdar, and C. Inzinger, "Application architecture for the Internet of cities: Blueprints for future smart city applications," *IEEE Internet Comput.*, vol. 20, no. 6, pp. 68–75, Nov./Dec. 2016.

[5] H. Farhangi, "The path of the smart grid," *IEEE Power Energy Mag.*, vol. 8, no. 1, pp. 18–28, Jan./Feb. 2010.

[6] X. Fang, S. Misra, G. Xue, and D. Yang, "Smart grid—The new and improved power grid: A survey," *IEEE Commun. Surveys Tuts.*, vol. 14, no. 4, pp. 944–980, 4th Quart., 2012.

[7] D. J. Cook, G. Duncan, G. Sprint, and R. L. Fritz, "Using smart city technology to make healthcare smarter," *Proc. IEEE*, vol. 106, no. 4, pp. 708–722, Apr. 2018.
[8] M. Mettler, "Blockchain technology in healthcare: The revolution starts here," in *Proc. IEEE 18th Int. Conf. e-Health Netw., Appl. Services (Healthcom)*, Sep. 2016, pp. 1–3.
[9] C. Sullivan and E. Burger, "E-residency and blockchain," *Comput. Law Secur. Rev.*, vol. 33, no. 4, pp. 470–481, Aug. 2017, doi: 10.1016/j.clsr.2017.03.016.
[10] e-Estonia. (2002). *e-Identity*. Accessed: May 15, 2019. [Online]. Available: https://e-estonia.com/solutions/e-identity/smart-id
[11] S. Ghosh, "Smart homes: Architectural and engineering design imperatives for smart city building codes," in *Proc. Int. Conf. Technol. Smart City Energy Secur. Power, Smart Solutions Smart Cities (ICSESP)*, 2018, pp. 68–72.
[12] F. Shrouf, J. Ordieres, and G. Miragliotta, "Smart factories in industry 4.0: A review of the concept and of energy management approached in production based on the Internet of Things paradigm," in *Proc. IEEE Int. Conf. Ind. Eng. Eng. Manage.*, Dec. 2014, pp. 697–701.
[13] S. Mekid and U. Baroudi, "Fastener tension monitoring system," U.S. Patent 8 893 557 B2, Nov. 25, 2014.
[14] H. Ohta and T. Sumigawa, "Bolt with function of measuring strain," U.S. Patent 7 293 466 B2, Nov. 13, 2007.
[15] J. D. Smith and S. G. Pothier, "Load sensing system including RFID tagged fasteners," U.S. Patent 7 412 898 B1, Aug. 19, 2008.
[16] C. E. Campanella, A. Cuccovillo, C. Campanella, A. Yurt, and V. M. N. Passaro, "Fibre Bragg Grating based strain sensors: Review of technology and applications," *Sensors*, vol. 18, no. 9, p. 3115, Sep. 2018, doi: 10.3390/s18093115.
[17] Y. Zhao, Y. Zhu, M. Yuan, J. Wang, and S. Zhu, "A laser-based fiber Bragg grating ultrasonic sensing system for structural health monitoring," *IEEE Photon. Technol. Lett.*, vol. 28, no. 22, pp. 2573–2576, Nov. 15, 2016.
[18] P. Giannelli, A. Bulletti, and L. Capineri, "Multifunctional piezopolymer film transducer for structural health monitoring applications," *IEEE Sensors J.*, vol. 17, no. 14, pp. 4583–4586, Jul. 2017.
[19] Y. Hu, C. Hong, Y. Zhang, and G. Li, "A monitoring and warning system for expressway slopes using FBG sensing technology," *Int. J. Distrib. Sensor Netw.*, vol. 14, no. 5, May 2018, doi: 10.1177/1550147718776228.
[20] BoltSafe, Beuningen, The Netherlands. (2019). *BoltSafe Sensor CMS. BoltSafe Sensor Continuous Monitoring System Datasheet, Version 2.0*. Accessed: Feb. 12, 2019. [Online]. Available: https://www.boltsafe.com/wp-content/uploads/2019/02/BoltSafe-Sensor-CMS-TechnicalDataSheet.pdf
[21] BoltSafe, Beuningen, The Netherlands. (2019). *BoltSafe Sensor PMS, BoltSafe Sensor Periodic Monitoring System Datasheet, Version 2.0*. Accessed: Feb. 12, 2019. [Online]. Available: https://www.boltsafe.com/wp-content/uploads/2019/02/BoltSafe-Sensor-PMS-TechnicalDataSheet.pdf
[22] C. Popenoe, "Making the case for tension indicating fasteners," *Amer. Fastener J.*, pp. 52–54, May/Jun. 2011.
[23] M. Sidorov, P. V. Nhut, A. Okubo, Y. Matsumoto, and R. Ohmura, "TenSense: IIoT enabled sensor node for remote measurement of a bolted joint tension," in *Proc. IEEE Int. Conf. Pervasive Comput. Commun.*, 2019, doi: 10.1109/PERCOM.2019.8767418.
[24] *LoRa Module Data Sheet, CMWX1ZZABZ-TEMP Datasheet*, Murata, Nagaokakyo, Japan, 2016.
[25] *Size and Power Optimized RPMA Module for the Machine NetworkTM, SARA-S200 Datasheet*, UBlox, Thalwil, Switzerland, 2017.
[26] *Sigfox/Sub-1GHz, WSSFM10R1AT Datasheet*, WISOL, Gyeonggi-Do, South Korea, 2018.
[27] *Digi Xbee Cellular NB-IoT, NB-IoT Cellular Smart Modem Preliminary Datasheet*, DIGI, Shah Alam, Malaysia, 2017.
[28] *Sub-GHz (868 or 915 MHz) Low Power Programmable RF Transceiver Modules, 6LoWPAN SPhSGRF Datasheet*, STMicroelectronics, Geneva, Switzerland, 2017.
[29] *CC2642R SimpleLinkTM Bluetooth 5 Low Energy Wireless MCU, CC2642R Datasheet*, Texas Instrum., Dallas, TX, USA, 2018.
[30] *PAN9320 Fully Embedded Stand-Alone Wi-Fi Module, Panasonic Wi-Fi Module Datasheet*, Panasonic, Kadoma, Japan, 2017.
[31] *NANO-S100 RPMA Module, NANO-S100 Datasheet*, UBlox, Thalwil, Switzerland, 2017.
[32] H. C. Lee and K. H. Ke, "Monitoring of large-area IoT sensors using a LoRa wireless mesh network system: Design and evaluation," *IEEE Trans. Instrum. Meas.*, vol. 67, no. 9, pp. 2177–2187, Sep. 2018.
[33] S. Mekid and B. Abdelhafid, "Bolt tension monitoring system," U.S. Patent 8 596 134 B1, Dec. 3, 2013.
[34] U. Baroudi and S. Mekid, "Bolt tension monitoring system," U.S. Patent 8 448 520 B1, May 28, 2013.
[35] S. Mekid, B. Abdelhafid, and U. Baroudi, "Smart lid for smart bolts and probes," U.S. Patent 8 540 468 B2, Sep. 24, 2013.
[36] H. Cao, S. K. Thakar, M. L. Oseng, C. M. Nguyen, C. Jebali, A. B. Kouki, and J.-C. Chiao, "Development and characterization of a novel inter-digitated capacitive strain sensor for structural health monitoring," *IEEE Sensors J.*, vol. 15, no. 11, pp. 6542–6548, Nov. 2015.
[37] *Low-Power Long Range LoRa Technology Transceiver Module, RN2903 Datasheet*, Microchip, Chandler, AZ, USA, 2018.
[38] *WM-SG-SM-42 LoRa Module, USI LoRa Datasheet*, Universal Sci. Ind. Shanghai Co., Ltd., Shanghai, China, 2017.
[39] *RFM95/96/97/98(W)—Low Power Long Range Transceiver Module, RFM95/96/97/98(W) Datasheet*, Shenzhen HOPE Microelectron. Co., Ltd, Shenzhen, China, 2017.
[40] *LoRaWAN 915MHz BAND TRX MODULE, 32001409 Datasheet*, Mipot, Cormons, Italy, 2018.
[41] *High Performance LoRaWANTM-RF-Modules and Sensors, FMLR-72-x-32L0 Datasheet*, Miromico, Zürich, Switzerland, 2018.
[42] *CW1276SL-915 Product Brief, CW1276SL Datasheet*, AcSiP, Taoyuan, Taiwan, 2018.
[43] *Dual-mode LoRa Module, LM-130H1 Datasheet*, GlobalSat, Boca Raton, FL, USA, 2017.
[44] X. Yang, E. Karampatzakis, C. Doerr, and F. Kuipers, "Security vulnerabilities in LoRaWAN," in *Proc. ACM/IEEE Int. Conf. Internet Things Design Implement. (IoTDI)*, Apr. 2018, pp. 129–140.
[45] L. M. Feeney, C. Rohner, P. Gunningberg, A. Lindgren, and L. Andersson, "How do the dynamics of battery discharge affect sensor lifetime?" in *Proc. IEEE/IFIP 11th Annu. Conf. Wireless Demand Netw. Syst. Services (WONS)*, Apr. 2014, pp. 49–56.
[46] K. Furset and P. Hoffman, "High pulse drain impact on CR2032 coin cell battery capacity," Nordic Semicond. ASA, Oslo, Norway, Energizer Holdings, Maryville Univ., St. Louis, MO, USA, Tech. Rep., 2011.
[47] Murata, Nagaokakyo, Japan. (2019). *Coin Manganese Lithium Dioxide Batteries, CR1632 Datasheet*. Accessed: Feb. 18, 2019. [Online]. Available: https://www.murata.com/en-us/products/productdata/8801520189470/CR1632.pdf?1550844009000
[48] C.-C. Lee, T.-Y. Chen, P.-H. Wu, and C.-T. Chen, "Three-factor control protocol based on elliptic curve cryptosystem for universal serial bus mass storage devices," *IET Comput. Digit. Techn.*, vol. 7, no. 1, pp. 48–56, Jan. 2013.

MICHAIL SIDOROV received the B.Sc. degree in informatics from Coventry University, U.K., in 2009, the B.Sc. degree in informatics engineering from Klaipeda University, Lithuania, in 2010, and the M.Sc. degree in embedded computing systems (EMECS) from the Norwegian University of Science and Technology (NTNU), Norway, and the University of Southampton (UoS), U.K., in 2013. He is currently pursuing the Ph.D. degree with the Toyohashi University of Technology, Japan, working in the field of the IoT. He was a Teaching Fellow and also the Laboratory Officer at the University of Southampton Malaysia, from 2013 to 2017. His current research interests include energy harvesting sensor networks, LPWAN, and blockchain technology for the IoT.

PHAN VIET NHUT received the B.Sc. degree from the Department of Civil Engineering, Danang University of Technology, Vietnam. He is currently a Lecturer with the Danang University of Technology, Vietnam, and also a graduate student with the Toyohashi Unversity of Technology, Japan. His research field is the applications of FRPs to civil structures, the development of repair and strengthening for steel structures using CFRP, and the strengthening of FRP connection using thin FRP sheets.

YUKIHIRO MATSUMOTO received the B.E., M.E., and Dr. Eng. degrees from the Toyohashi University of Technology, Japan, in 2002, 2004, and 2007, respectively.

He is currently an Associate Professor with the Department of Architecture and Civil Engineering, Toyohashi University of Technology. His research field is the fiber-optic sensing for FRP material, the applications of FRPs to civil structures, and the development of repair and strengthening for steel structures using CFRP. He is the winner of the Best Paper Award, Japan Reinforced Plastics Society (JRPS), in 2012. He is a member of the International Institute for FRP in Construction (IIFC), the International Association for Shell and Spatial Structures (IASS), the Japan Society of Civil Engineers (JSCE), the Architectural Institute of Japan (AIJ), and the Japan Society of Steel Construction (JSSC).

REN OHMURA received the bachelor's degree in electric engineering, the master's degree in computer science, and the Ph.D. degree from Keio University, in 1999, 2001, and 2004, respectively. He is currently a Lecturer with the Department of Computer Science and Engineering, Toyohashi University of Technology, Japan. He currently runs Ubiquitous Systems Laboratory, TUT, and supervises students ranging from B.Sc. to Ph.D. level. His research works are on ubiquitous computing, wearable computing, the IoT, smart environment, battery-less systems, and distributed systems.